A Source and Ground Motion Study of the Veracruz Earthquakes of 29 October 2009 (Mw5.7) and 4 August 2021 (Mw4.8): Evidence of Strong Azimutual Variation of Attenuation

A. Iglesias[1], S. K. Singh[1], D. Arroyo[2], X. Pérez-Campos[1,3], V. H. Espíndola[1], A. Vargas[4], F. Córdoba-Montiel[5] and Deni M. González-López[6]

Abstract

We study two moderate earthquakes that occurred offshore the State of Veracruz, in the southwestern Gulf of Mexico, on 29 October 2009 (M_w 5.7) and 4 August 2021 (M_w 4.8). The former was located near the town of Alvarado and latter near the city of Veracruz. The events were well recorded by accelerographs and seismographs at local and regional distances. *W*-phase regional centroid moment tensor inversion reveals that they had reverse-faulting mechanism, similar to several other earthquakes in the southwestern Gulf of Mexico. Of the seven focal mechanisms now available along the southwestern margin, two are strike slip and the rest are of thrust type, suggesting a heterogeneous stress regime. We take advantage of local and regional recordings produced by these two earthquakes to study the characteristics of the ground motion. Source spectra computed at each station separately (without correcting for the site effect), assuming a reasonable geometrical spreading and $Q = 141f^{0.63}$, show remarkably high variability due to difference in path and local site effects. The geometric mean apparent source spectrum (source spectrum including site effects) of both earthquakes may be modeled by an ω^2-Brune source model with a stress drop, $\Delta\sigma$, of 40 MPa. These source spectra, along with the application of stochastic method, yield peak ground acceleration (*PGA*) and velocity (*PGV*) as a function of distance in general agreement with the observations. Of greater practical importance is the ground motion at sedimentary sites in the city of Veracruz and at the Laguna Verde Nuclear Power Plant (LVNPP) site, especially from a postulated M_w 6.5 earthquake which is a reasonable scenario event for the region. For the city of Veracruz and LVNPP we estimate site effect with respect to the ω^2-Brune source with $\Delta\sigma$ of 2 MPa. There is some support for this $\Delta\sigma$. We apply both stochastic and empirical Green's functions (*EGF*) techniques in the estimation of the ground motion. The recording of the 2021 earthquake is taken as the *EGF*, and $\Delta\sigma$ of the *EGF* and the target event are assumed to be the same and equal to 2 MPa. The predicted *PGA* and *PGV* at sedimentary sites in the city of Veracruz and LVNPP above the hypocenter (depth = 20 km) from the postulated M_w 6.5 earthquake are 0.2 g and 10 cm/s and 0.18 g and 3 cm/s, respectively. These results are preliminary as they are based on several assumptions.

Resumen

En este trabajo estudiamos dos sismos de magnitud moderada que ocurrieron frente a las costas del Estado de Veracruz, en el suroeste del Golfo de México, el 29 de octubre de 2009 (M_w 5.7) y el 4 de agosto de 2021 (M_w 4.8). El primero estaba ubicado cerca de Alvarado, Ver. y el segunda cerca de la ciudad de Veracruz, Ver. Ambos eventos fueron bien registrados mediante acelerógrafos y sismógrafos a distancias locales y regionales. La inversión del tensor de momento con fase W muestra mecanismos de falla inversa, similar a otros sismos en el suroeste del Golfo de México. De los siete mecanismos focales disponibles a lo largo del margen suroeste, dos muestran fallas de deslizamiento lateral y el resto muestran mecanismos de tipo inverso, lo que sugiere un régimen de tensiones heterogéneo. Con base en los registros locales y regionales de estos dos sismos, en este trabajo, estudiamos las características del movimiento del suelo. Los espectros de la fuente calculados en cada estación por separado (sin corregir el efecto de sitio), suponiendo una dispersión geométrica razonable y $Q = 141f^{0.63}$, muestran una variabilidad notablemente alta debido a la diferencia en los efectos de la trayectoria y del sitio. La media geométrica del espectro de fuente aparente (espectro de fuente que incluye los efectos del sitio) de ambos terremotos puede modelarse mediante un modelo de fuente ω^2-Brune con una caída de esfuerzos, $\Delta\sigma$, de 40 MPa. A través de un método estocástico, los espectros de la fuente producen aceleraciones máximas del suelo (PGA) y velocidades máximas (PGV), con respecto de la distancia, que en general están de acuerdo con las observaciones. De importancia relevante son las aceleraciones en sitios en la ciudad de Veracruz y en el sitio de la Central Nuclear Laguna Verde (LVNPP), especialmente suponiendo un terremoto postulado de M_w 6.5, lo cual es un escenario razonable para la región. Para la ciudad de Veracruz y LVNPP estimamos los efectos de sitio asumiendo una fuente ω^2-Brune con $\Delta\sigma$ de 2 MPa, caída de esfuerzos que tiene cierto soporte. En este trabajo fueron aplicados métodos tanto de funciones de Green (EGF) estocásticas como empíricas en la estimación del movimiento del suelo. El registro del sismo de 2021 se toma como EGF, y se supone que las $\Delta\sigma$'s del EGF y el evento objetivo son las mismas e iguales a 2 MPa. Los PGA y PGV pronosticados en sitios sedimentarios en la ciudad de Veracruz y la LVNPP sobre el hipocentro (profundidad = 20 km) del sismo postulado de M_w 6.5 son 0.2 g y 10 cm/s y 0.18 g y 3cm/s, respectivamente. Estos resultados son preliminares ya que se basan en varios supuestos.

* Corresponding author: Arturo Iglesias, **arturo@igeofisica.unam.mx**
[1] Instituto de Geofísica, Universidad Nacional Autónoma de México, Mexico City, Mexico.
[2] Departamento de Materiales, Universidad Autónoma Metropolitana, Mexico City, Mexico.
[3] CTBTO Preparatory Comission, Vienna, Austria.
[4] Instituto de Ingeniería, Universidad Veracruzana, Veracruz, Veracruz, Mexico.
[5] Centro de Ciencias de la Tierra, Universidad Veracruzana, Xalapa, Veracruz, Mexico.
[6] Posgrado en Ciencias de la Tierra, UNAM, Mexico City, Mexico.

Arturo Iglesias Mendoza, Shri Krishna Singh, Danny Arroyo, Xyoli Pérez Campos, Víctor Hugo Espíndola Castro, Alejandro Vargas Colorado, Francisco Córdoba-Montiel and Deni M. González-López.

Introduction

Seismicity in the central and northern Gulf of Mexico is low. Consequently, there are only a few studies that deal with this topic. An earthquake on 24 July 1978 (m_b 5), which occurred in this part of the gulf, was analyzed by Frohlich (1982). A sequence of three earthquakes (M_w 4.6, 5.2, 5.9) that occurred in 2006 near the 1978 event was studied by Nettles (2006) and Gangopadhyay and Sen (2008). Location and focal mechanism of the 1978 and 10 September 2006 (M_w 5.9) earthquakes are shown in Figure 1. Origin of these earthquakes has been attributed to the stress caused of deposition of sediments carried by the Missisipi river (Frohlich, 1982; Gangopadhyay and Sen, 2008).

Seismicity is more abundant along the southwestern margin of the gulf (Suárez and López, 2015). The largest known earthquake in this region, the Jaltipan earthquake, occurred on 26 August 1959 (M_w 6.4) causing serious damage to the towns of Jaltipan, Coatzacoalcos, and Minatitlan (Figueroa, 1964; Rosenblueth, 1964; Reséndiz, 1964). As seen in Figure 1, the southwestern gulf earthquakes have either a thrust faulting or a strike-slip focal mechanism. Trend of P axes of the thrust earthquakes has been explained by strong coupling along the subduction plate interface offshore Tehuantepec and absolute motion of the north American plate (e.g., Dewey and Suárez, 1991; Suárez, 2000; Suárez and López, 2015; Singh *et al.*, 2015). The strike-slip earthquake of 15 February 2017 (M_w 4.3) whose mechanism was also determined in this study (Appendix A) may be related to left-lateral movement on the Neogene Veracruz fault studied in detail by Adreani *et al.* (2008). However, there is no structure with which we can relate the strike-slip event of 23 May 2007 (M_w 5.7).
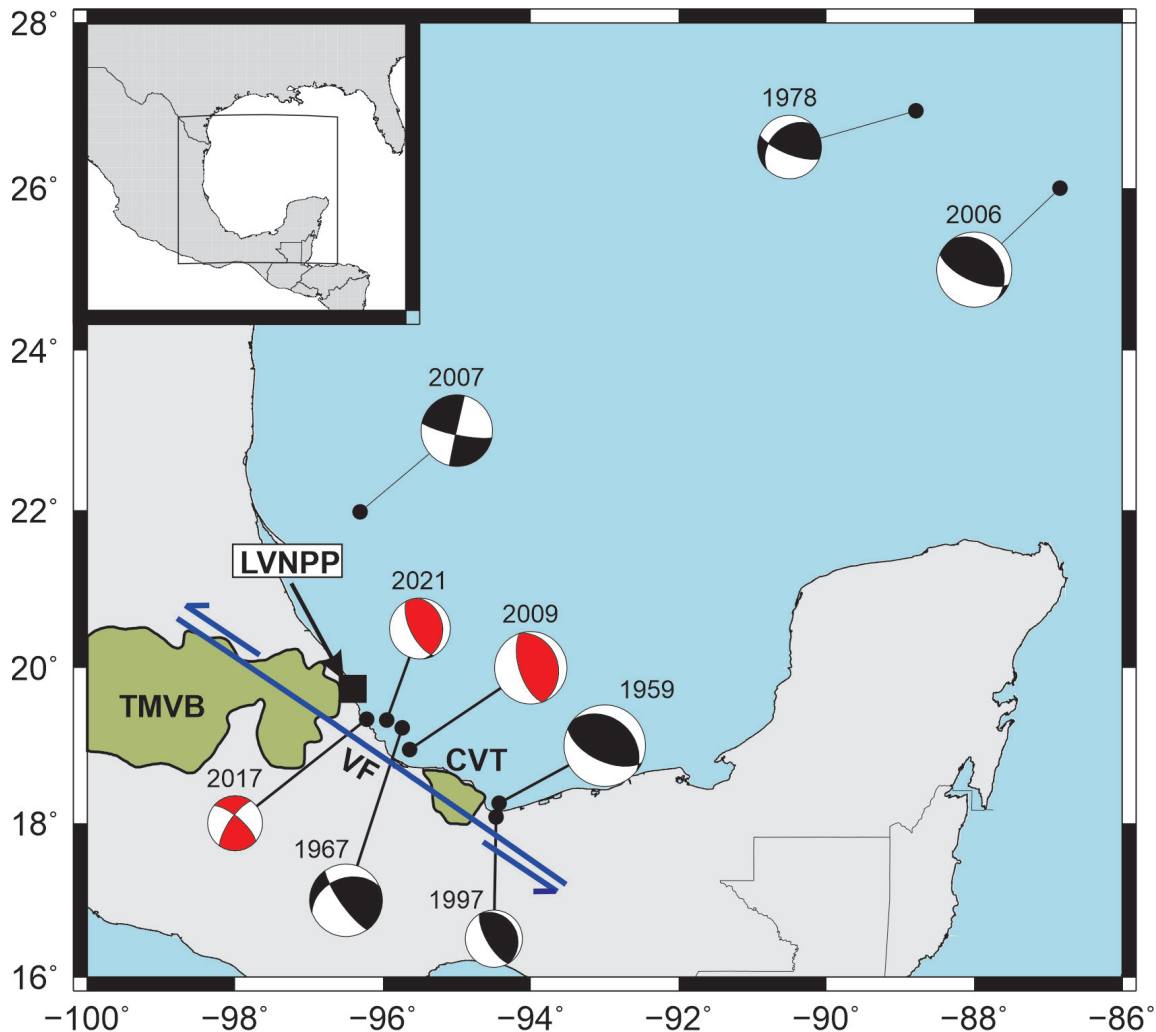
Figure 1. Map of Gulf of Mexico showing location of earthquakes with known focal mechanism. Red and white beach balls are focal mechanisms obtained in this study using local and regional recordings. LVNPP: Laguna Verde Nuclear Power Plant. VF: Veracruz fault (Adreani *et al.*, 2008). Focal mechanism of 2017 event is consistent with the geologically-mapped sense of motion on the Veracruz fault. Note that the earthquakes along the southwest margin of the gulf have thrust as well as strike-slip mechanism.

As more focal mechanisms have become available, our understanding of the current deformation and the geodynamics of the gulf has improved. However, there is still no study dealing with expected ground motion from postulated local and regional earthquakes, occurring at the southwestern margin of the gulf, mostly because of the scarcity of recordings. This is an important shortcoming as there are several important cities and towns along the coast of southwestern Gulf of Mexico (e.g., Veracruz, Alvarado, Coatzacoalcos, and Minatitlan), as well as hydrocarbon exploration and production facilities, and the Laguna Verde Nuclear Power Plant (LVNPP) (Figure 1). The region is exposed to seismic hazard from intraslab earthquakes in the subducted Cocos plate and those that occur along the southwestern margin of the gulf. Indeed, in the seismic design of the

LVNPP, the ground motion from a migrating M_w 6.5 earthquake was of primary concern. In view of the 1959 Jaltipan event, an M_w 6.5 earthquake near the coast of the gulf is a likely scenario event for the region.

Seismic instrumentation in the state of Veracruz presently consists of stations of the Servicio Sismológico Nacional (SSN, National Seismological Service, Mexico) at the LVNPP (named LVIG) and Tuzandepetl (named TUIG). They are equipped with broadband seismograph and accelerograph. These stations have been in operation since 1996 (LVIG) and 1992 (TUIG). Federal Electricity Commission (CFE) maintains accelerographs and seismographs in and near the LVNPP and Universidad Veracruzana (UV) operates a few accelerographs and seismographs in and near the city of Veracruz (Figures 2 and 3).

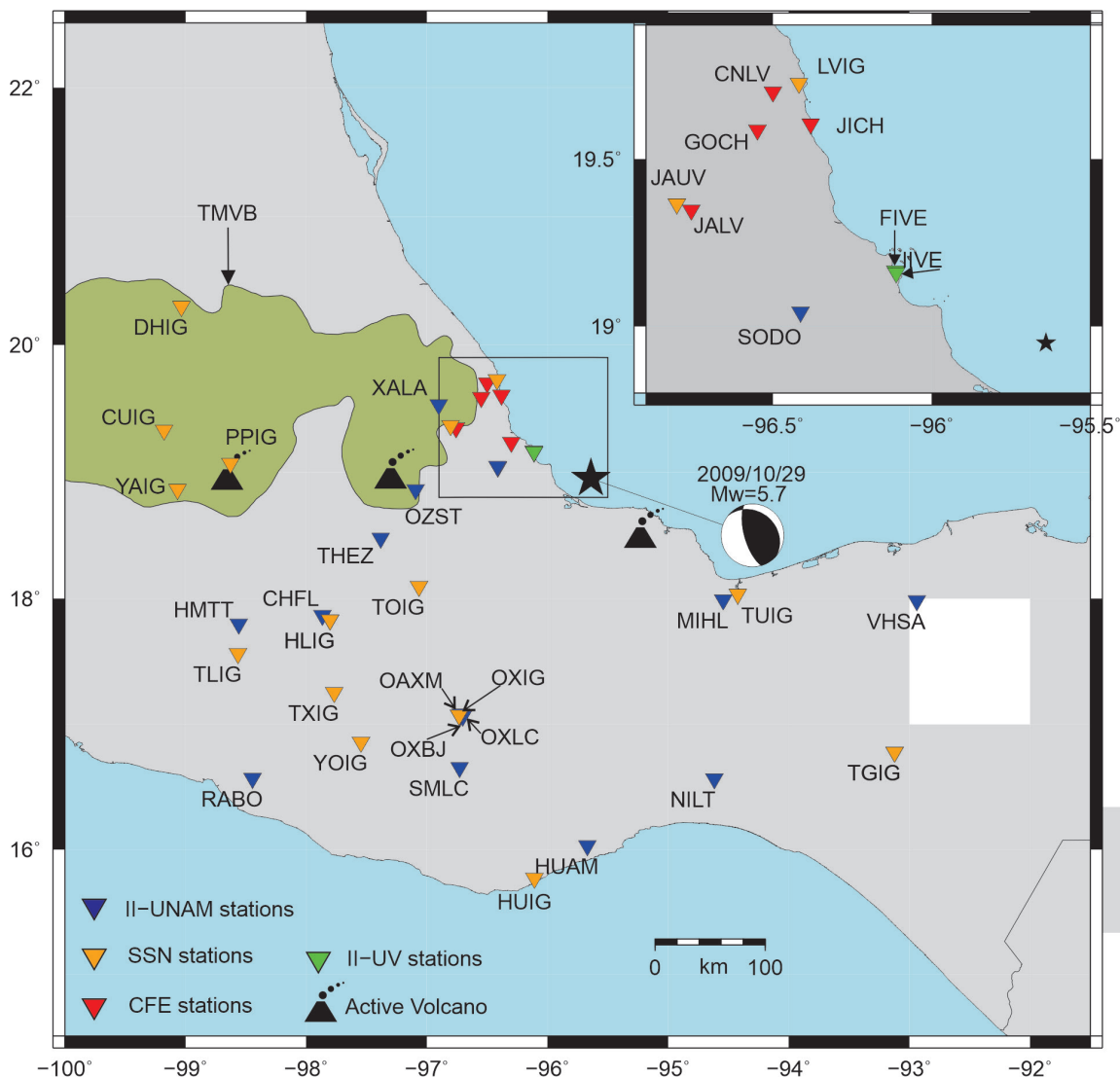

Figure 2. Location and focal mechanism of the 2009 Alvarado earthquake and stations whose recordings are analyzed in this study. Black triagle: active volcano. Green area: Trans Mexican Volcanic Belt. Inset: an enlarged area near the source.

Figure 3. Location and focal mechanism of the 2021 Veracruz earthquake and stations whose recordings are analyzed in this study. Black triagle: active volcano. Green area: Trans Mexican Volcanic Belt. Inset: an enlarged area near the source.
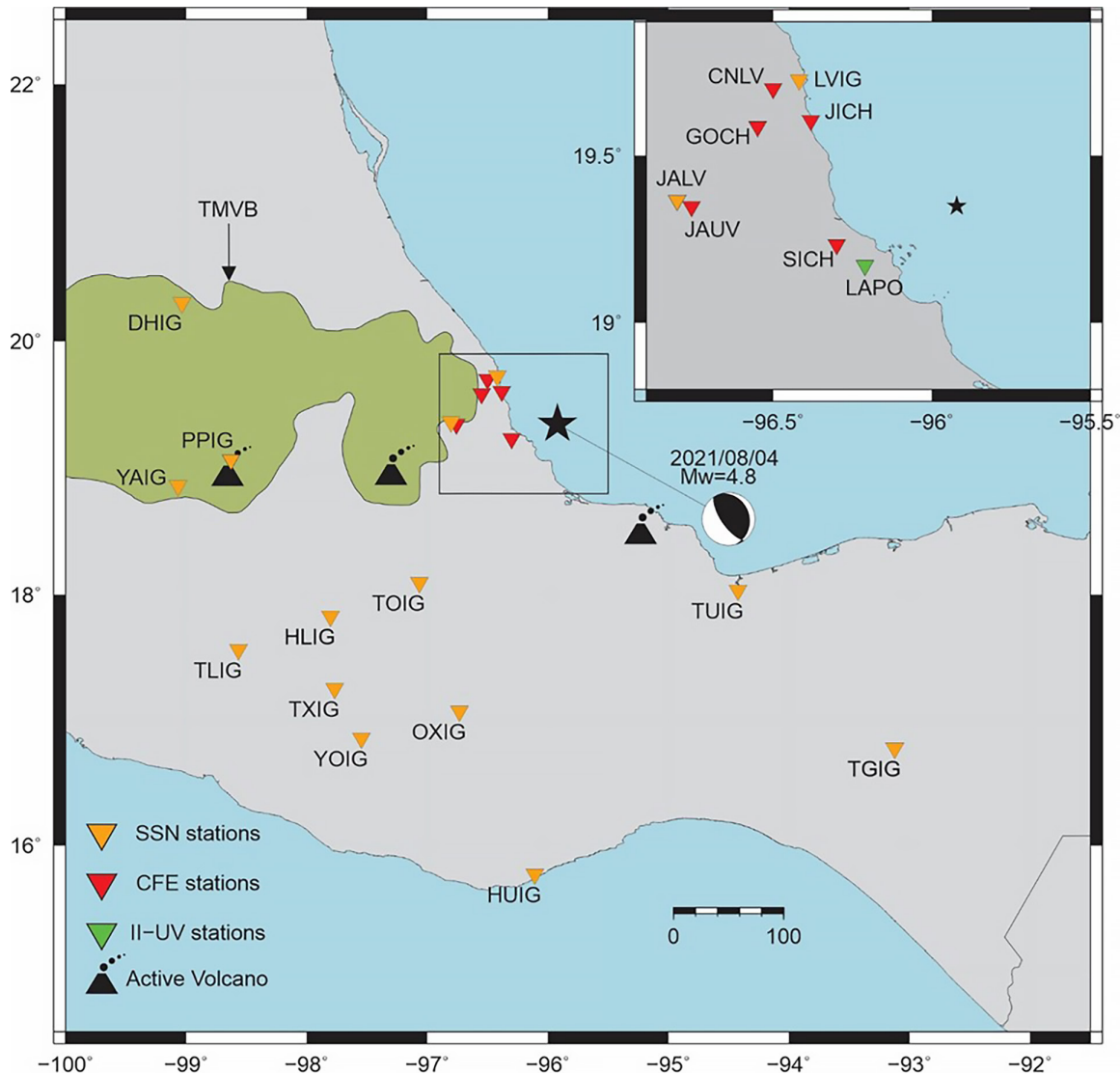
Recently, two moderate earthquakes have been fairly-well recorded, permitting us to determine their source parameters and to obtain a preliminary estimate of ground motion from postulated earthquakes based on the analysis of the local and regional recordings. Alvarado earthquake of 29 October 2009 (M_w5.7) was recorded by 3 accelerographs in and near the city of Veracruz (distance < 100 km), many stations of the SSN network, and the accelerographic network operated by Instituto de Ingeniería, UNAM at farther distances (Figure 2). Veracruz earthquake of 4 August 2021 was recorded by 8 near-source stations (distance < 100 km) and by many stations at regional distances (Figure 3). The accelerograms were corrected for instrument response by multiplication with a constant whereas the broadband seismograms were corrected using information on poles and zeros. We use the recordings of the two earthquakes to perform *W*- phase centroid moment tensor inversion. Both earthquakes involved reverse faulting. The recordings of the events (distance ≤ 400 km) reveal a surprisingly large variability of the ground motion, suggesting dramatic difference in the path to individual stations and the local site effect. We investigate whether the geometric mean of the apparent source spectrum (source spectrum including the site effect) of both events may be modelled by an ω^2-Brune source (Brune, 1968) and whether PGA and PGV estimated from the application of stochastic method are in reasonable agreement with the observations. We focus on the important and practical issue of the estimation of ground motion at sedimentary sites in and near the city of Veracruz and at LVNPP site from postulated earthquakes along the southwestern margin of the gulf, applying stochastic and empirical Green´s function techniques. We pay special atten-

tion to the expected motions from a future M_w 6.5 earthquake, a scenario event for the region.

Location of the Earthquakes

The velocity model used in locating the 2009 and 2021 earthquakes is given in Table 2. In this model, the *P* wave velocities and depths of the layers above Moho are taken from Singh *et al.* (2015) where appropriate references are given. The velocities and depths of the layers below Moho are taken from the model routinely used by the SSN. The depth of the events in the location were unstable. In locating the 2009 earthquake we fixed the depth at 27 km. This depth was determined by Suárez and López (2015) from the inversion of teleseismic *P* waves. For the 2021 earthquake the depth was fixed at 16 km which was obtained from *W*-phase inversion (see next section). Table 1 gives the location of the events. We also located an event which occurred on 15 February 2017 near the 2021 earthquakes. A detailed analysis of the event is given in Appendix A.

Table 1. Source parameters of earthquakes in and near Gulf of Mexico.

No.	Date	Location	Depth	M_w		Focal Mechanism		
		°N	°W	km		φ °	δ °	λ °
1	26 Aug 1959[a]	18.26	94.43	21	6.4	309	32	102
2	11 Mar 1967[b]	19.23	95.74	26	5.7	250	39	20
3	24 Jul 1978[c]	26.49	88.79	15	5.0	225	49	111
						240	63	52
4	06 Sep 1997[d]	18.08	94.47	30	4.5	330	20	90
5	10 Sep 2006	26.32	86.84	30	5.9	324	28	117[e]
6	23 May 2007	21.98	96.31	24	5.6	102	80	-1[e]
		(22.02	96.27	11	5.6	95	71	-16)[f]
		(21.98	96.14	44	5.5	106	83	8)[g]
		(22.0	96.3	6.7	5.6	97	80	3)[h]
7	29 Oct 2009	19.005	95.602	27	5.7	162	64	90[i]
		(19.14	95.58	17	5.7	164	69	10)[e]
		(18.9	95.8	16	4.8	153	65	81

[a] Location from ISS; depth, focal mechanism, and M_w from Suárez (2000).
[b] Location from ISC; depth, focal mechanism, and M_w from Suárez (2000).
[c] Location, depth, and focal mechanism from Frohlich (1982). The two mechanisms are extreme types consistent with first-motion data.
[d] Singh *et al.* (2015).
[e] Global CMT catalog.
[f] Source parameters listed in **http://www.eas.slu.edu/eqc/eqc_mt/MECH.NA/20070523190916/index.html**
[g] Franco *et al.* (2013).
[h] Suárez and López (2015).
[i] All parameters from this study; location from phase data with depth fixed at 27 km; M_w and focal mechanism from *W*-phase inversion.
[j] All parameters from this study; location from phase data; M_w and focal mechanism from regional centroid moment tensor inversion (see Appendix A).
[k] All parameters from this study; location from phase data with depth fixed at 16 km; M_w and focal mechanism from *W*-phase inversion.

Table 2. Crustal model used in the location of 2009 Alvarado and 2021 Veracruz earthquakes. Ratio of *P*-wave to *S*-wave speed has been taken as 1.78.

Layer	Thickness, km	*P*-wave speed α, km/s
1	1.8	2.80
2	15.6	4.25
3	15.6	6.5
4	67.0	7.25
5	∞	7.95

Centroid Moment Tensor Inversion

Since 2014, the SSN has implemented a routine calculation of M_w through W-phase inversion (Kanamori and Rivera, 2008). It uses an algorithm modified for moderate magnitude earthquakes by Hayes *et al.* (2009) and revised by Duputel *et al.* (2012). The algorithm is automatically triggered for $M \geq 5.2$ earthquakes ten minutes after the origin time and uses the broadband data from stations of the SSN (Pérez-Campos *et al.*, 2019). It starts with the SSN location and magnitude, and looks for the best half duration and then the best location. Later, the solution is manually revised to eliminate data with problems (e.g., inverse polarity or glitches) or a bad fit given the preferred solution.

Figure 4 shows the revised W-phase solution for the 29 October 2009 (M_w 5.7) and the 4 April 2021 (M_w 4.8) events and the fit of the inversion. For these events, 28 and 13 channels, filtered from 0.0067 to 0.02 Hz, were used in the inversions. The corresponding stations were located between 185 and 810 km
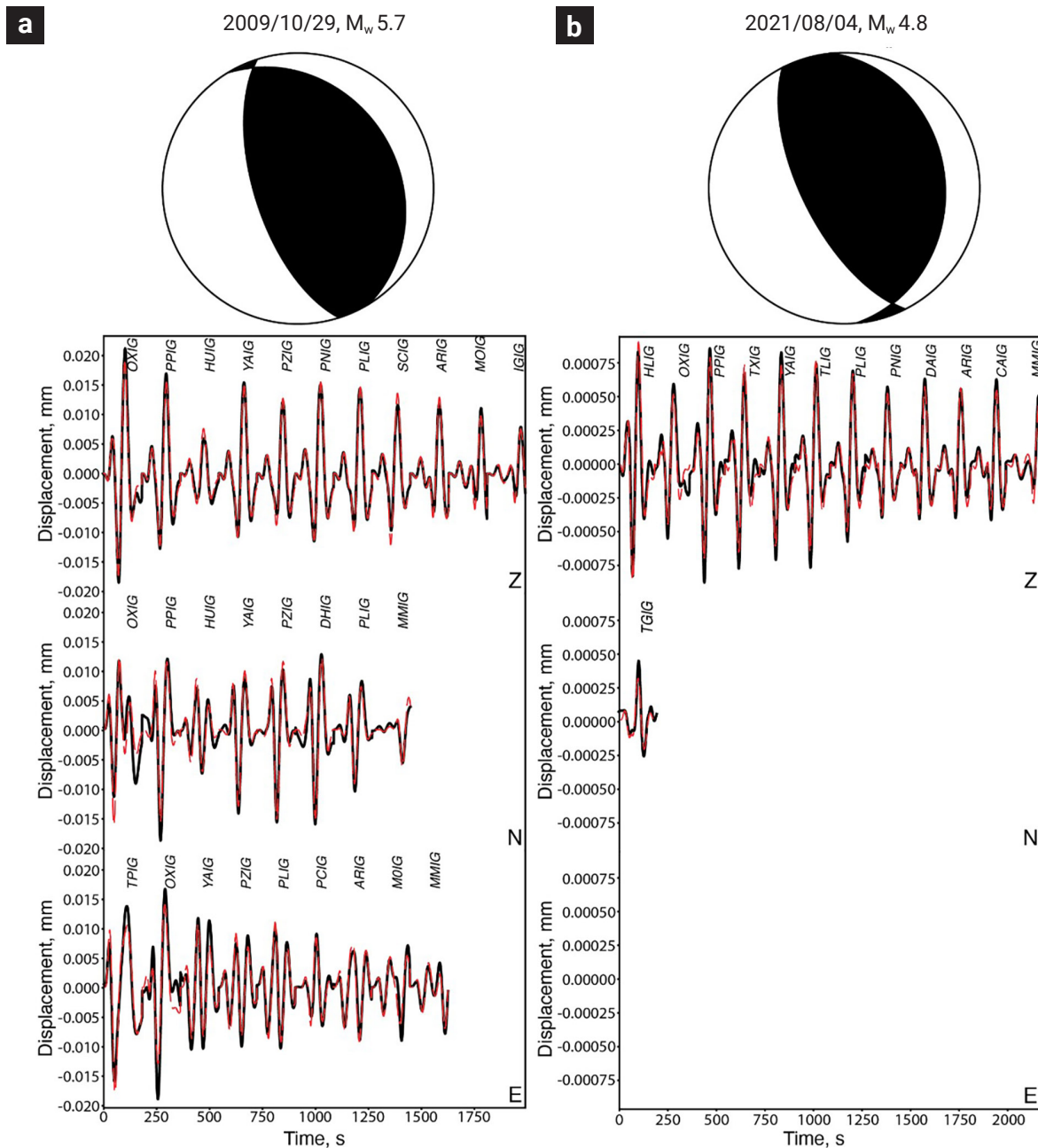

Figure 4. *W*-phase solution of a) 29 October 2009, M_w 5.7 and b) 4 August 2021, M_w 4.8 earthquakes. Top: Focal mechanism solution. Bottom: *W*-phase fit for the three components (Z = vertical; N = North; E = East). The black and red dashed traces correspond to the synthetic *W* phase for the preferred solution and the observed *W* phase, respectively.

from the epicenter for the 2009 earthquake, and 240 and 775 km for the 2021 event. The depths of the 2009 and 2021 events returned by the *W*-phase inversion are 19.5 km and 15.5 km, respectively. The seismic moments are $M_0 = 5.07 \times 10^{17}$ Nm and $M_0 = 1.93 \times 10^{16}$ Nm. The focal mechanisms, which in both cases correspond to an reverse-faulting, are listed below:

2009 earthquake
Nodal plane 1: $\varphi_1 = 328.7°$, $\delta_1 = 26.8°$, $\lambda_1 = 77.7°$
Nodal plane 2: $\varphi_2 = 162.4°$, $\delta_2 = 63.9°$, $\lambda_2 = 90.2°$
2021 earthquake
Nodal plane 1: $\varphi_1 = 354.6°$, $\delta_1 = 26.5°$, $\lambda_1 = 109.3°$
Nodal plane 2: $\varphi_2 = 153.2°$, $\delta_2 = 65.1°$, $\lambda_2 = 80.7°$

The focal mechanisms of the 2009 and 2021 events are very similar. While *W*-phase mechanism of the 2009 event is also similar to that reported in the Global CMT catalog, it differs considerably from that reported by Suárez and López (2015) (Table 1).

Centroid moment tensor inversion of the relatively small earthquake (M_w 4.3) of 15 February 2017 is discussed in Appendix A.

Source Spectrum

Moment rate spectrum, $\dot{M}_0(f)$, of an earthquake can be estimated from the Fourier amplitude spectrum of the recorded ground motion. The method requires corrections for the diminution and amplification of seismic waves as they travel from the source to the recording site. Ideally, $\dot{M}_0(f)$ estimated at different stations should be similar. Generally, however, they differ because the corrections are inadequate to account for the complex and varying path and local site effects. On the other hand if $\dot{M}_0(f)$ is known or specified, then the Fourier spectrum at any site can be estimated. The stochastic method may, then, be applied to estimate ground-motion parameters useful in earthquake engineering (e.g., Boore, 1983).

A brief description of the theory follows. Under far-field, point-source approximation, Fourier amplitude spectrum of the horizontal component of acceleration of an event at a distance R, $A(f, R)$, may be written as:

$$A(f, R) = C \cdot G(R) \, [\{f^2 \dot{M}_0(f)\} S(f)][\, e^{-\pi f R/\beta Q(f)}] \tag{1}$$

where,

$$S(f) = Site(f) \, e^{-\pi \kappa f} B(f), \tag{2}$$

$$C = FPR_{\theta\varphi}(2\pi)^2/(4\pi\rho\beta^3) \tag{3}$$

In equations above, $\dot{M}_0(f) \rightarrow M_0$ as $f \rightarrow 0$, R = hypocentral distance, $R_{\theta\varphi}$ = average radiation pattern (0.55), F = free surface amplification (2.0), P takes into account the partitioning of energy in the two horizontal components ($1/\sqrt{2}$), β = shear-wave velocity at the source, ρ = density in the focal region, and $Q(f)$ = quality factor, which includes both anelastic absorption and scattering. The attenuation in the near-surface layer and the finite bandwidth of the observed spectrum are accounted by the parameter κ (Singh *et al.*, 1982; Anderson and Hough, 1984) and/or the Butterworth filter, B(f) (Boore, 1983). Often either κ or $B(f)$ is sufficient to explain the high-frequency falloff of the spectrum. We assume the geometrical spreading term, $G(R)$, in equation (1) as $1/R$ for $R \leq 100$ km and $1/(100R)^{0.5}$ for R > 100 km.

We take $Q(f) = 141 f^{0.63}$ estimated for the eastern and central Trans Mexican Volcanic Belt (Canas, 1986; Singh *et al.*, 2017). β and ρ in the source region are assumed to be 3.75 km/s and 2.85 gm/cm^3, respectively. We take logarithm of equation (1):

$$log \, [A(f, R)] = log \, C + log \, G(R) + log \, [f^2 \dot{M}_0(f) \, S(f)] - [1.36\{Rf/\beta Q(f)\}]$$

and compute $log \, [f^2 \dot{M}_0(f) S(f)]$ at each station. Plots of $[f^2 \dot{M}_0(f) S(f)]$ at each station for the earthquakes of 2009 are shown in Figure 5a. The corresponding geometric mean and $\pm$ one standard deviation curves are plotted in Figure 5b. The spectra, grouped in three distance ranges, $62 < R < 160$ km, $165 < R < 285$ km, and $290 < R < 390$ km, are illustrated in Figures 5c,d, and e. These figures reveal surprisingly large variability of ground motion (especially at $f \geq 3$ Hz), suggesting large difference in $S(f)$ of each site. The variability persists in each distance group. The sites with especially anomalous spectrum are identified in the figure. These sites are LVNPP, PPIG (Popocatépetl volcano) and DHIG (Demacu) (Figure 2).

As it is not possible to determine $S(f)$ at each site, we do not attempt to separate $S(f)$ from $[f^2 \dot{M}_0(f) S(f)]$. Our goal here is not to determine the true source spectrum; we seek a spectrum that can be used in the estimation of ground motion from future earthquakes via the stochastic method. For this purpose, the path- and site-affected source acceleration spectrum, $[f^2 \dot{M}_0(f) S(f)]$, henceforth also called the apparent source acceleration spectrum, $ASAS(f)$, suffices. $S(f)$ in equation 2 may be written as:

$$S(f) = ASAS(f) / f^2 \dot{M}_0 S(f) \tag{4}$$

We interpret the geometric mean $ASAS(f)$ by the ω^2-source model of Brune (1970). Figure 5b shows theoretical source

spectra corresponding to M_0 of 5.07×10^{18} Nm (M_w 5.7) and of 40, 10, and 2 MPa. The observed geometric mean $ASAS(f)$ is well approximated by a $\Delta\sigma$ of 40 MPa. We reiterate that this is not the true stress drop but one that fits the $ASAS(f)$.

Figure 6 is similar to Figure 5 but for the 2021 Alvarado earthquake. Similar to 2009 earthquake, it also reveals large variability of $ASAS(f)$ at individual sites (Figure 6a) that persists in each of the three distance ranges (Figures 6c,d, and e). There are some sites with especially anomalous spectrum e.g., IIVE, FIVE, LVIG, PPIG, TUIG, DHIG. The sites with especially anomalous spectrum for the 2021 event show the same tendency

as observed for the 2009 earthquake. The geometric mean of $ASAS(f)$ is, again, reasonably well fit by the ω^2-source model with M_0 of 1.93×10^{16} Nm (M_w 4.8) and M_0 of 40 MPa (Figure 6b).

Clearly, we need more recordings at local and regional distances of the earthquakes that occur near the coast of Veracruz to learn whether the ω^2-source model with $\Delta\sigma$ of 40 MPa is good approximation to $ASAS(f)$ of most of such events. Lacking such dataset, we shall assume that this is so. Replacing $[f^2\dot{M}_0(f) S(f)]$ in equation 1 by the Brune ω^2-source model with M_0 of 40 MPa, we may estimate the Fourier acceleration spectrum at an "average" site ($R \leq 400$ km).
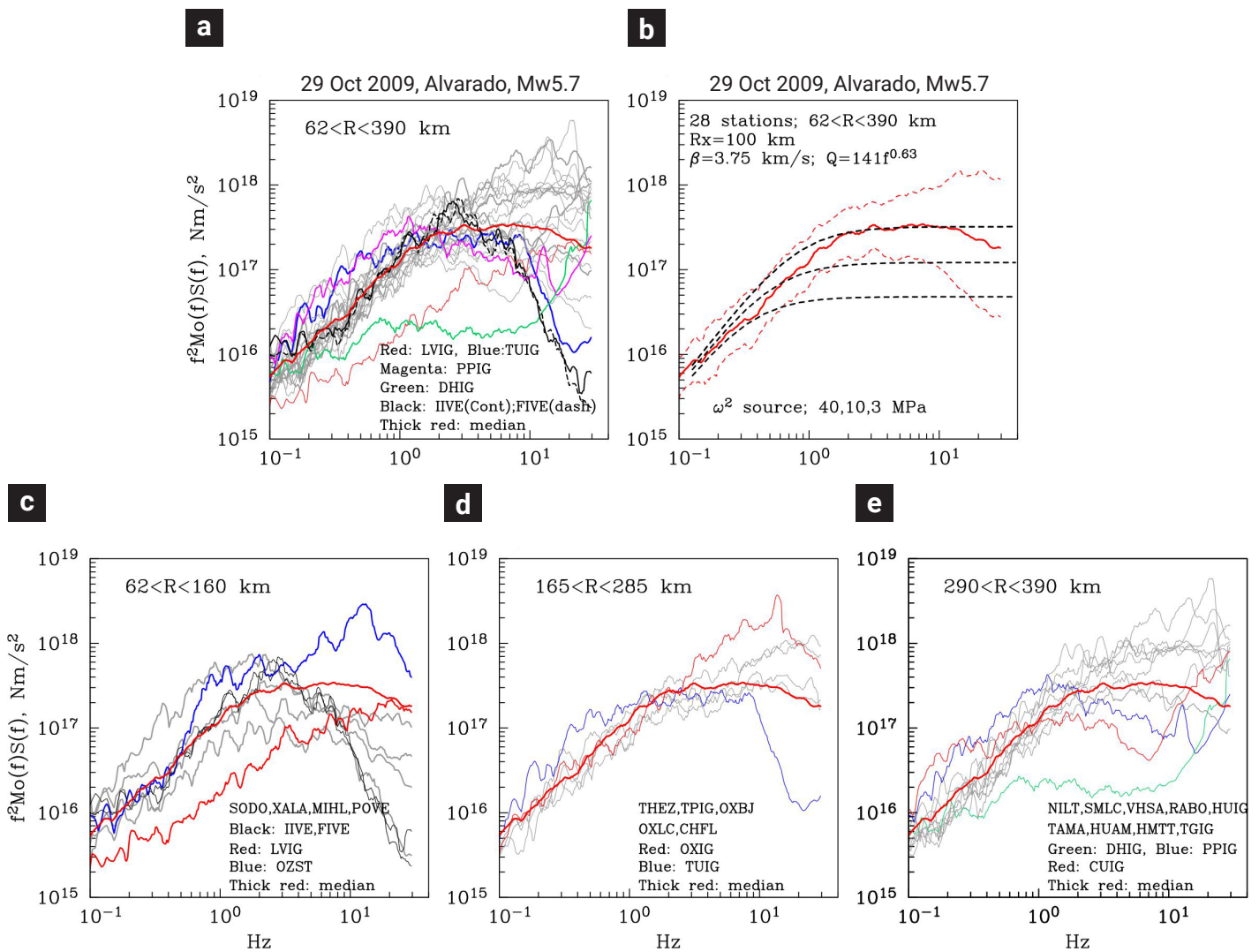

Figure 5. a) $ASAS(f) = [f^2\dot{M}_0(f)S(f)]$ curves of the 2009 earthquake estimated at individual stations. The plot shows remarkable variability. Especially anomalous sites (IIVE, FIVE, OXIG, OZST, LVIG, PPIG, and DHIG) are identified. Thick red curve shows the plot of the geometric mean. b) Geometric mean and $\pm$ one standard curves. Superimposed are theoretical curves for an ω^2-Brune source model with $\Delta\sigma$ of 40, 10, and 3 MPa. The observed geometric mean curve is well fit with $\Delta\sigma$ of 40 MPa. c), d), e) $ASAS(f)$ curves with stations grouped in three distant ranges. For reference, each frame shows the geometric mean curve (Figure 5b).
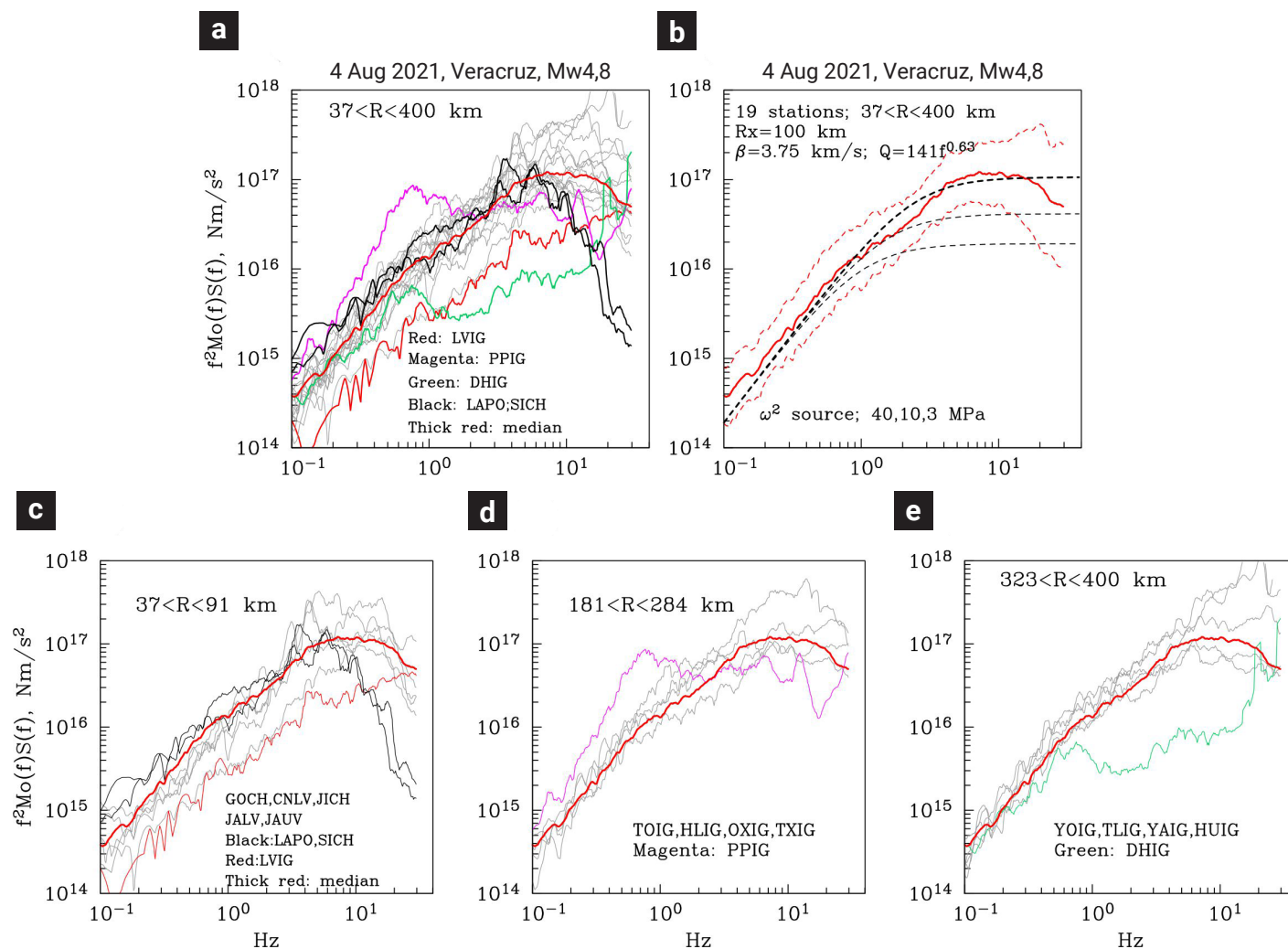
Figure 6. Same as Figure 5 but for the 2021 earthquake. Anomalous sites in this case are LAPO and SICH, and, similar to the 2009 event, the sites of LVIG, PPIG, and DHIG. Similar to the 2009 earthquake, the observed geometric mean curve of the 2009 event is well fit by an ω^2-Brune source with $\Delta\sigma$ of 40 MPa. For reference, each frame shows the geometric mean curve (Figure 6b).

Observed and Predicted Ground Motions from the Two Veracruz Earthquakes

We verify whether $A(f,R)$ computed for a Brune source with $\Delta\sigma$ of 40 MPa , along with the application of the stochastic method, gives *PGA* and *PGV* values consistent with those observed during the 2009 and 2021 earthquakes. A parameter needed in the application of the method is the duration of intense part of the ground motion, T, which we take as $T = 1 / f_c + 0.05R + C$, where R is in km, f_c is the corner frequency, and C is a constant. This relation was originally proposed by Herrmann (1985) with C equals 0. For the Brune source model $f_c = 0.49 \beta (\Delta\sigma/M_0)^{1/3}$. $\Delta\sigma$ is taken as 40 MPa. Based on an earlier analysis of a sequence of small earthquakes in Morelia, Mexico (Singh *et al.*, 2012) we set $C = 3$ sec. The predicted curves and observed

PGA and *PGV* values of the two earthquakes (Tables 3 and 4) are shown in Figure 7. We note that the values at site DHIG are especially low. Ignoring DHIG, the predicted *PGA* and *PGV* curves fit the observed values reasonbly well. Most of the values fall within a factor of two of the predicted curves. Presumably, the same set of parameters and application of the stochastic method would produce reasonable PGA and PGV curves for postulated earthquakes. To keep the work to a manageable level, we abstained from testing the sensitivity of the results to other choices of the parameters. We did, however, test the sensitivity of the predictions to the critical parameter of stress drop. We performed calculations with twice and half of the stress drop of 40 Mpa: 80 MPa and 20 MPa. The values, with respect to those for 40 MPa, were greater by a factor of ~1.5 and smaller by a factor of ~1/1.5 for higher and lower stress drops, respectively.

Table 3. PGA and PGV, Alvarado Earthquake, 29 October 2009, M_w5.7.

Station	R,km	PGA, cm/s²			PGV, cm/s			Site
		NS	EW	Z	NS	EW	Z	
IIVE	62	22.8	19.1	10.6	9.86E-01	1.19	3.63E-01	S
FIVE	63	23.9	19.2	16.2	1.41	1.03	6.74E-01	S
SODO	90	4.87	4.68	5.35	2.23E-01	2.47E-01	1.71E-01	A
LVIG	120	2.68	4.17	2.58	7.30E-02	7.77E-02	4.60E-02	H
XALA	150	2.02	1.93	1.61	1.21E-01	1.20E-01	7.48E-02	H
OZST	160	15.5	11.6	8.07	2.48E-01	2.23E-01	1.73E-01	S
MIHL	161.3	3.28	3.27	1.46	3.73E-01	3.45E-01	1.44E-01	S
TUIG	167	1.98	1.87	8.65E-01	1.66E-01	1.38E-01	7.30E-02	S
THEZ	199	2.23	2.93	2.48	1.17E-01	1.47E-01	6.24E-02	H
TPIG	199	1.51	1.37	1.71	8.69E-02	8.62E-02	7.17E-02	H
OXIG	246	2.7	4.06	2.47	7.21E-02	1.26E-01	5.59E-02	H
OXBJ	246	1.63	1.19	1.83	4.18E-02	3.48E-02	4.77E-02	H
OXLC	246	1.38	1.63	7.62E-01	6.07E-02	7.44E-02	3.97E-02	H
OAXM	246	6.33	5.5	3.72	1.73E-01	2.11E-01	9.37E-02	A
CHFL	271.3	4.52E-01	4.57E-01	3.42E-01	2.39E-02	2.91E-02	2.88E-02	H
SMLC	287.3	1.05	1.08	6.68E-01	7.22E-02	4.78E-02	3.78E-02	H
NILT	291	2.05	1.86	6.15E-01	5.89E-02	8.65E-02	3.39E-02	H
VHSA	304.2	1.22	9.86E-01	3.28E-01	8.79E-02	4.73E-02	1.94E-02	S
RABO	305.2	2.87E-01	4.22E-01	3.54E-01	2.12E-02	2.40E-02	2.19E-02	H
PPIG	314	2.96E-01	3.11E-01	2.09E-01	4.71E-02	4.64E-02	2.01E-02	H
TAMA	322.1	5.52E-01	5.17E-01	3.52E-01	3.08E-02	3.62E-02	2.78E-02	H
HUAM	330.2	6.85E-01	6.20E-01	5.39E-01	2.89E-02	2.91E-02	2.14E-02	H
TLIG	340	4.74E-01	3.35E-01	3.37E-01	2.37E-02	1.77E-02	2.11E-02	H
HMTT	341.1	4.44E-01	5.41E-01	3.93E-01	3.60E-02	3.66E-02	4.14E-02	H
TGIG	361	1.42	8.91E-01	5.20E-01	8.89E-02	6.96E-02	4.43E-02	H
HUIG	363	4.18E-01	3.02E-01	2.41E-01	1.73E-02	1.12E-02	1.40E-02	H
CUIG	379	6.40E-02	6.48E-02	5.76E-02	1.95E-02	2.19E-02	1.25E-02	H
DHIG	389	1.48E-02	1.28E-02	1.84E-02	5.16E-03	5.05E-03	5.93E-03	H

Site S: soft, A: Alluvium, H: rock

Table 4. PGA and PGV, Veracruz Earthquake, 4 August 2021, M_w4.8

| Station	R,km	PGA, cm/s²	PGV, cm/s	Site					
		NS	EW	Z	NS	EW	Z		
LAPO	36.6	29.5	23.7	20.8	7.65E-01	1.25E+00	4.13E-01	S	
SICH	41.7	21.2	13.1	7.64	7.89E-01	6.00E-01	1.89E-01	S	
JICH	56.8	5.99	2.67	4.48	1.06E-01	7.03E-02	1.23E-01	H	
LVIG	67.7	2.2	2.78	4.84	2.75E-02	4.14E-02	3.12E-02	H	
GOCH	70.8	18.1	14.9	5.45	3.12E-01	3.51E-01	1.00E-01	H	
CNLV	72.6	7.19	5.59	9.34	7.25E-02	5.34E-02	8.06E-02	H	
JALV	86.5	6.69	11.5	10.5	2.01E-01	3.11E-01	1.63E-01	H	
JAUV	91.2	19.4	11.7	8.26	5.28E-01	2.37E-01	1.66E-01	H	
TOIG	181.5	1.14E+00	9.08E-01	1.03E+00	2.66E-02	2.37E-02	3.75E-02	H	
TUIG	216.6	1.76E-01	1.24E-01	1.48E-01	5.30E-03	5.19E-03	2.78E-01	S	
HLIG	257.5	1.44E-01	1.63E-01	1.38E-01	4.74E-03	5.74E-03	4.31E-03	H	
OXIG	264.7	4.87E-01	7.13E-01	4.85E-01	1.38E-02	3.06E-02	1.16E-02	H	
TXIG	282	1.58E-01	1.72E-01	1.43E-01	9.93E-03	8.48E-03	6.31E-03	H	
PPIG	283.5	1.09E-01	9.76E-02	4.70E-02	1.71E-02	1.39E-02	6.20E-03	H	
YOIG	323	9.12E-02	8.70E-02	7.10E-02	5.03E-03	5.58E-03	4.01E-03	H	
YAIG	332.3	5.90E-02	5.23E-02	3.57E-02	3.89E-03	3.25E-03	2.34E-03	H	
TLIG	339.3	1.07E-01	9.44E-02	9.13E-02	4.28E-03	5.15E-03	5.57E-03	H	
DHIG	340.8	8.30E-03	6.33E-03	7.66E-03	1.27E-03	1.16E-03	1.00E-03	H	
HUIG	396.3	9.43E-02	8.51E-02	5.34E-02	2.69E-03	2.73E-03	2.43E-03	H	

Site S: soft, A: Alluvium, H: rock
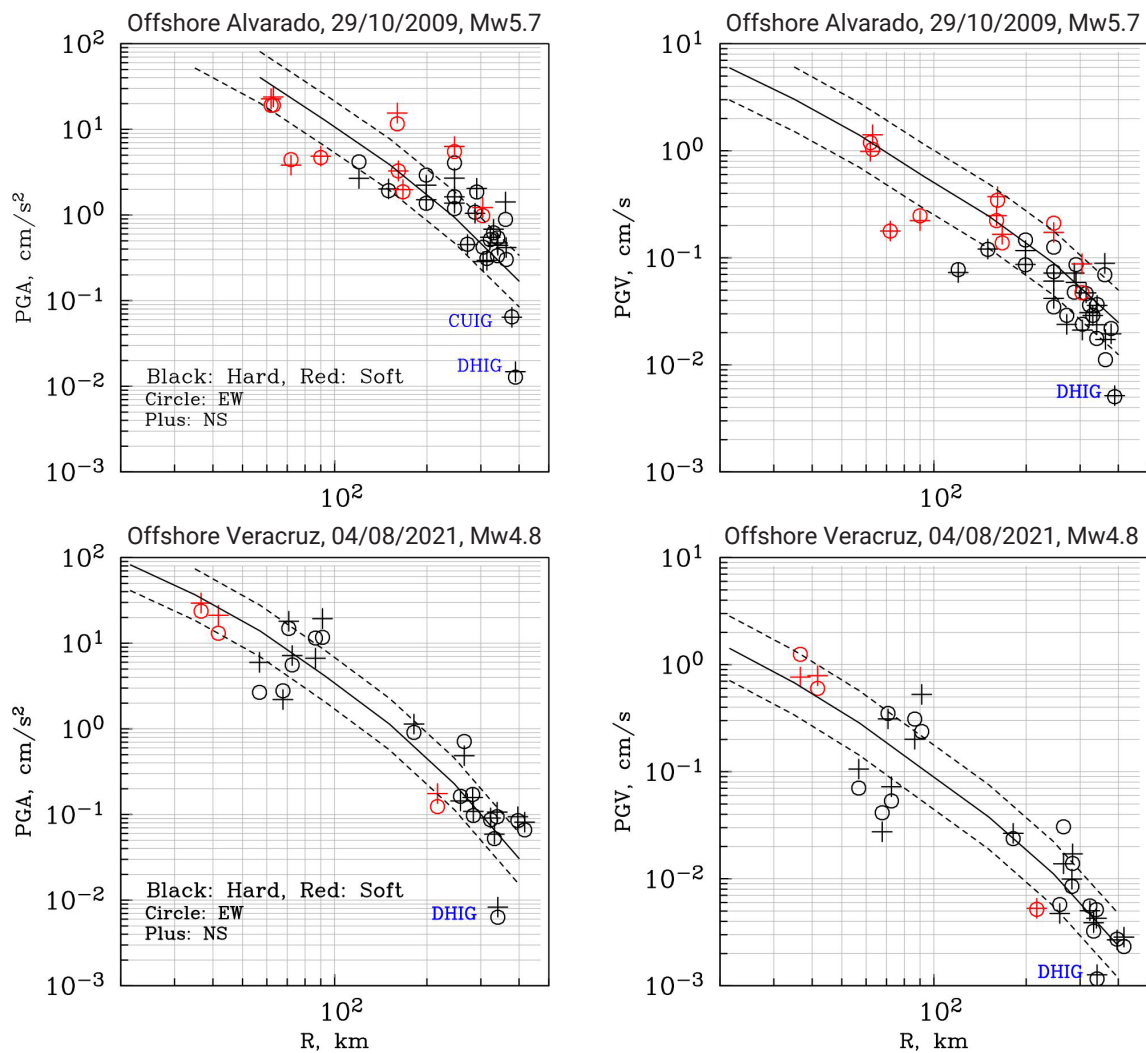
Figure 7. Comparison of observed and stochastically simulated PGA and PGV values for the 2009 Alvarado earthquake (top two frames) and the 2021 Veracruz earthquake (bottom two frames).

Ground Motion in the city of Veracruz and Laguna Verde Nuclear Power Plant from Postulated Earthquakes

The stochastic predictions above are for an "average" site located at $R \leq 400$ km. Of practical interest, however, is the ground motion in the near-source region, especially at sedimentary sites in and near the city of Veracruz and at the LVNPP. We focus our attention to these sites and take recourse to both empirical Green function (EGF) and stochastic methods.

a) EGF Method

We synthsize ground motion from an M_w 6.5 event using the recordings of 2021 earthquake (M_w 4.8) as empirical Green's functions (EGF). A method proposed by Ordaz *et al.* (1995) is used in the synthesis. It is based on adding N scaled EGF records, each differed in time by a random delay. The probability distribution of the delays is such that, on an average, the simulations follow an ω^2-spectral scaling at all frequencies. The method requires specification of the seismic moment, M_0, and the stress drop, $\Delta\sigma$, of both the EGF and the target earthquakes. In our case, M_0 of the EGF is 1.93×10^{15} N-m (M_w 4.8) and that of the target event is 7.08×10^{18} N-m (M_w 6.5). Unfortunately, the site effect distorts the source spectrum so that it is difficult to estimate the corner frequency, f_c, hence $\Delta\sigma$, of the EGF.

We explored the possibility of estimating f_c of the 2021 earthquake from the spectral ratios of the aftershocks to the mainshock, thus eliminating the site effect. The aftershocks of the 2021 earthquake were not large enough to produce useful recordings. However, we could find an aftershock of the 2009 earthquake

which was well recorded at four broadband stations (LVIG, TPIG, OXIG, PPIG) (Figure 2). The source parameters of this aftershock, listed in SSN catalog, are: 29/10/2009; 23:25:20.3; 18.95^0N, -95.71^0E; depth = 24 km; M 4.3. The location of the aftershock is close to that of the 2009 mainshock. The focal mechanism of the aftershock could not be determined because of complex crustal structure and poor signal at long period. Here we assume that the aftershock and mainshock were collocated and had similar mechanism. Under these assumptions, the spectral ratio of the aftershock to mainshock at the same station

provides the ratio of the source spectra. These ratios are shown in Figures 8 where all three components are plotted. At $f \leq 1$ Hz the ratios are ~10-2, *i.e.*, M_0 of the aftershock is 5.07×10^{15} Nm (M_w 4.4). Superimposed on the observed spectral ratios are theoretical ratios corresponding to the ω^2-source model (see Chael, 1987 for the equation of theoretical ratio) and $f_c = 0.3$ Hz ($\Delta\sigma = 2$ MPa) and $f_c = 0.5$ Hz ($\Delta\sigma = 10$ MPa). Two relationships between $\Delta\sigma$ and M_0 are considered: (1) $\Delta\sigma$ is constant, and (2) $\Delta\sigma$ increases with M_0 such that $\Delta\sigma$ is proportional to $M_0^{1/4}$ (a scaling proposed by Nuttli, 1983 for mid-plate earthquakes; see
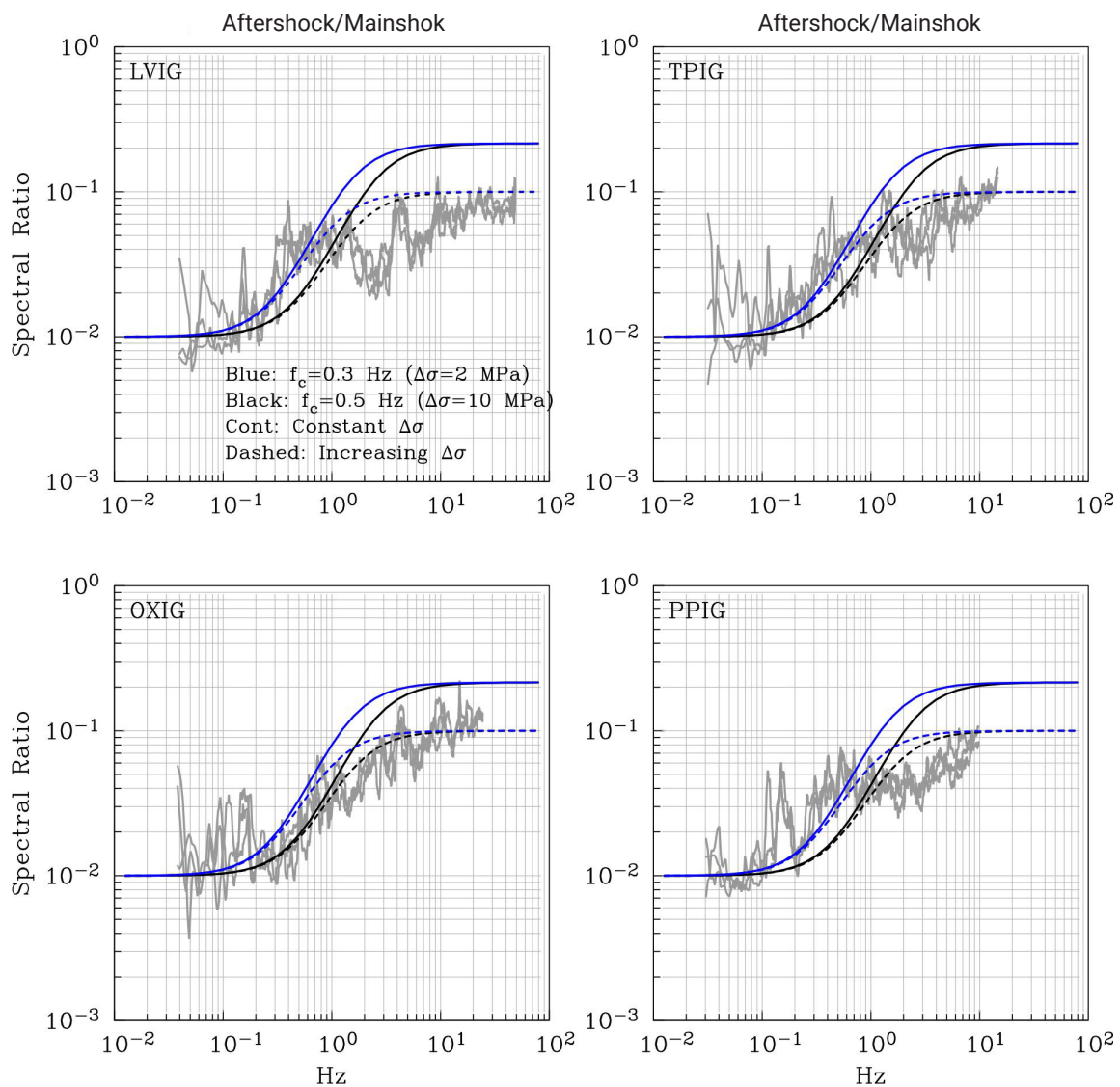

Figure 8. Spectral ratios of an aftershock to the 2009 Alvarado mainshock at the same station. All three components are plotted. At $f \leq 1$ Hz the ratios are ~10-2, *i.e.*, M_0 of the aftershock is 5.07×10^{15} Nm (M_w 4.4). Superimposed on the observed spectral ratios are theoretical ratios corresponding to the ω^2-source model and $f_c = 0.3$ Hz ($\Delta\sigma = 2$ MPa) and $f_c = 0.5$ Hz ($\Delta\sigma = 10$ MPa). Two relationships between $\Delta\sigma$ and M_0 are considered: 1) $\Delta\sigma$ is constant, and 2) $\Delta\sigma$ increases with M_0 such that $\Delta\sigma$ is proportional to $M_0^{1/4}$. Theoretical ratios for $f_c = 0.3$ Hz better fit the observed spectral ratios at $f < 0.5$ Hz at LVIG, TPIG, and PPIG irrespective of the $\Delta\sigma$ - M_0 relationship. However, at OXIG, $f_c = 0.5$ Hz is preferable.

also Chael, 1987). Theoretical ratios for $f_c = 0.3$ Hz better fit the observed spectral ratios at $f < 0.5$ Hz at LVIG, TPIG, and PPIG irrespective of the $\Delta\sigma$- M_0 relationship. However, at OXIG, $f_c = 0.5$ Hz is preferable. Perhaps, a source directivity is the cause of the greater fc at OXIG. At $f > 1$ Hz the theoretical ratios for constant approximate the observed ratios very poorly; increasing stress drop model does a better job. Figure 8 and the discussion above support $f_c = 0.3$ Hz ($\Delta\sigma = 2$ MPa); certainly $f_c \geq 0.5$ Hz ($\Delta\sigma \geq 10$ MPa) appears unlikely. Stress drop of 2 MPa is close

to median stress drop of 4 MPa reported by Allman and Shearer (2009) in a global study of stress drop variation. We shall further assume that $\Delta\sigma$ of the EGF earthquake of 2021 and the target earthquake (M_w 6.5) is the same as that of the 2009 mainshock, i.e., 2 MPa. With these assumptions, *PGA* and *PGV* values were synthesized for the target event at the near-source sites where the 2021 earthquake was recorded using the EGF method. The results, along with those obtained from the stochastic method, are presented in the next section.
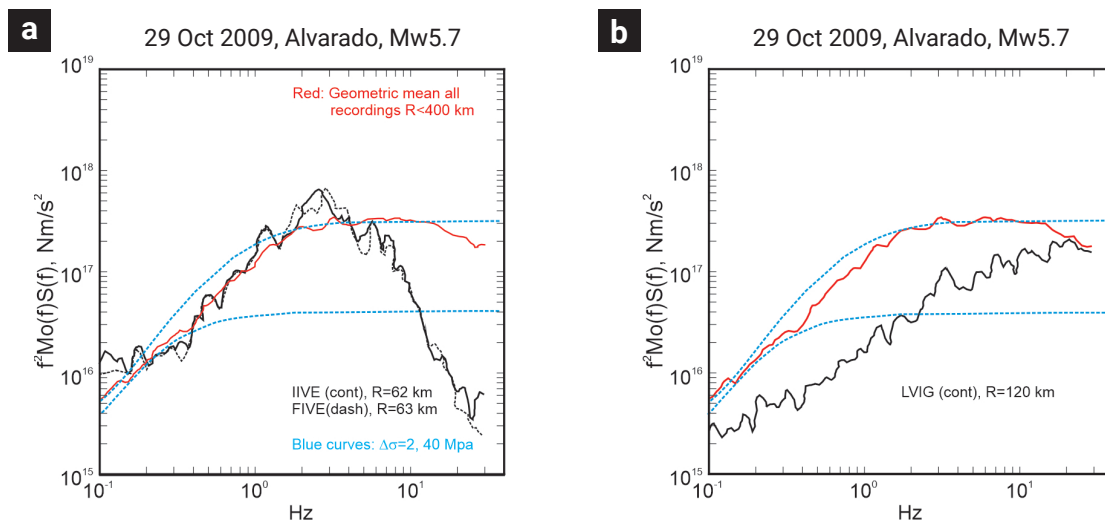

Figure 9. a) *ASAS(f)* of the 2009 earthquake at near-source sedimentary sites of IIVE and FIVE located in the city of Veracruz. b) Same as a) but for LVIG located in the LVNPP. Theoretical source spectra for an ω^2-Brune source with $\Delta\sigma$ of 40, and 2 MPa are shown for reference. Also shown in the figure is the geometric mean *ASAS(f)* computed from all recordings (R < 400 km) from Figure 5b.
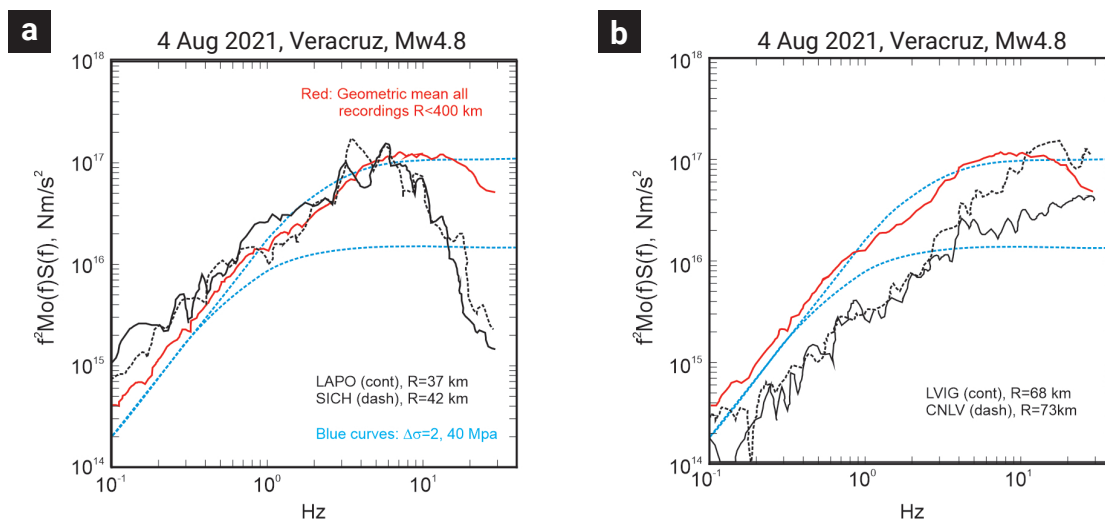

Figure 10. Same as Figure 9 but for the 2021 earthquake. LAPO and SICH are the sedimentary sites in the city of Veracruz. CNLV is a site in the LVNPP, near LVIG. The geometric mean *ASAS(f)* computed from all recordings (R < 400 km) is from Figure 6b.

b) Stochastic Method

Figure 9a shows the *ASAS(f)* of the 2009 earthquake at near-source sedimentary sites of IIVE and FIVE located in the city of Veracruz. Figure 9b illustrates a similar plot for LVIG located in the LVNPP. Theoretical source spectra for an ω^2 Brune source with $\Delta\sigma$ of 40, and 2 MPa are shown for reference. Also included in the figure is the geometric mean *ASAS(f)* computed from all recordings (Figure 5b). This spectrum fits those at IIVE and FIVE at *f* less than about 3 Hz; the spectra, however, rapidly falloff above 3 Hz. We attribute the falloff to unaccounted attenuation of seismic waves in the sedimentary upper layers.

The spectrum at LVIG is remarkable; it is lower than at other sites, except DHIG (Figure 5); it is also lower than the theoretical source spectrum corresponding to $\Delta\sigma = 2$ MPa. The expected merger of theoretical and LVIG spectra at low frequencies (~ 0.1 Hz) does not occur and there is no spectral falloff at least till *f* = 20 Hz.

Figure 10 is similar to Figure 9 but for the 2021 earthquake. LAPO and SICH are the near-source stations on sedimentary sites in the city of Veracruz. Similar to 2009 earthquake, the source spectra at these sites rapidly falloff at frequencies greater than 3 Hz. At LVNPP, the earthquake was recorded at LVIG and a nearby site CNLV. The *ASAS(f)* at LVIG and CNLV are similar at *f* < 4 Hz; both are lower than the theoretical spectrum corresponding to $\Delta\sigma = 2$ MPa. Above 4 Hz, the CNLV spectrum deviates from the LVIG spectrum; the former becomes greater than the latter, most probably as a consequence of low-velocity superficial layer. We address the peculiar nature of the spectra at LVIG and CNLV in a later section.

Assuming that the true source spectrum is given by the theoretical ω^2-source model with $\Delta\sigma$ of 2 MPa, the deviation of the observed *ASAS(f)* from this spectrum may be attributed to *S(f)*. Figure 11a shows geometric mean of the *ASAS(f)* at IIVE and FIVE for the 2009 earthquake and the corresponding theoretical spectrum. Figure 11b illustrates the observed *ASAS(f)* at LVIG as well as the theoretical source spectrum. Figures 11c, and d give similar plots for the 2021 earthquake. From equation 4, *S(f)* during the earthquakes of 2009 and 2021 at sedimentary sites in the city of Veracruz and sites at LVPP are given in Figures 11e and f, respectively. It may be noted that the *S(f)* of the two earthquakes are fairly similar. Knowing $[f^2\dot{M}_0(f)S(f)]$, the acceleration spectrum, $A(f, R)$, may be computed (equation 1) and the stochastic method may be used to obtain ground motion parameters.

Predicted *PGA* curves, using the stochastic method, for M_w 4.5, 5.5, and 6.5, as function of *R*, for sedimentary Veracruz sites and LVNPP sites are illustrated in Figures 12a and c, respectively. The corresponding *PGV* curves are given in Figures 12b and d. Observed *PGA* and *PGV* values during the 2009 (red plusses)

and 2021 earthquakes (blue plusses) are superimposed on these figures. For the LVNPP sites, the synthesized *PGA* and *PGV* values for a scenario M_w 6.5 earthquake, using the recordings of the 2021 (M_w 4.8) earthquake as EGFs, are very similar to the stochastically predicted ones. For the sedimentary sites in the city of Veracruz, the EGF predictions are greater than the stochastic ones. We checked the stochastic predictions for stress drops of 4 and 10 MPa instead of 2 MPa. A 5 times increase in $\Delta\sigma$ produces ~ 3 time increase in PGA and PGV values. A two-fold increase in $\Delta\sigma$ produces ~ 1.6 time increase in PGA and PGV values while a five times greater $\Delta\sigma$ produces ~ 3 times larger PGA and PGV values. This shows the sensitivity of the results to the stress drop of the postulated earthquake. In as much as $\Delta\sigma$ of the postulated event is uncertain by a factor of at least 2 or 3 of 2 MPa, the predicted values of PGA and PGV values corresponding to $\Delta\sigma$ of 2 MPa may be off by a factor of 2 or more.

As mentioned earlier, the estimation of ground motion from a scenario M_w 6.5 earthquake is of great practical interest, especially above the hypocenter (R ~ 20 km). For such an event the stochastically predicted *PGA* and *PGV* at sedimentary coastal sites above the hypocenter are 0.18 g and 10 cm/s. At LVNPP, the corresponding predicted motions are 0.2 g and 3 cm/s. As mentioned above, the values may be off by a factor of atleast 2.

Unusual Recordings at DHIG and LVIG Sites

Two sites where *ASAS(f)* is unusually low are DHIG and LVIG (Figures 2 and 3). Here we briefly discuss the cause of this extraordinary observation.

Shapiro *et al.* (2000) noted that the amplitude of seismic waves traversing the active Popocatépetl volcano before reaching Mexico City is diminished by a factor of about one-third at frequencies greater than 1 Hz as compared to those that do not cross it. The higher attenuation below the volcano was attributed to the presence of magma and partial melting of rocks. DHIG is a limestone site at the northern end of the Mexican Volcanic Belt (MVB) (Figures 2 and 3). The wavepaths from 2009 and 2021 earthquakes to DHIG do not cross any active volcano but travel about 300 km in the MVB (Figures 2 and 3). Greatly reduced *ASAS(f)* at DHIG is very likely a consequence low *Q* along the path. Relatively low *Q* in the MVB has been reported by Singh *et al.* (2007).

Singh *et al.* (2006) documented a relative diminution of amplitude of seismic waves recorded at LVIG during certain group of earthquakes. They associated the diminution to wavepath through low-*Q* mantle wedge. LVIG, situated in the LVNPP facility, is located on basaltic flows underlain by vulcanites that
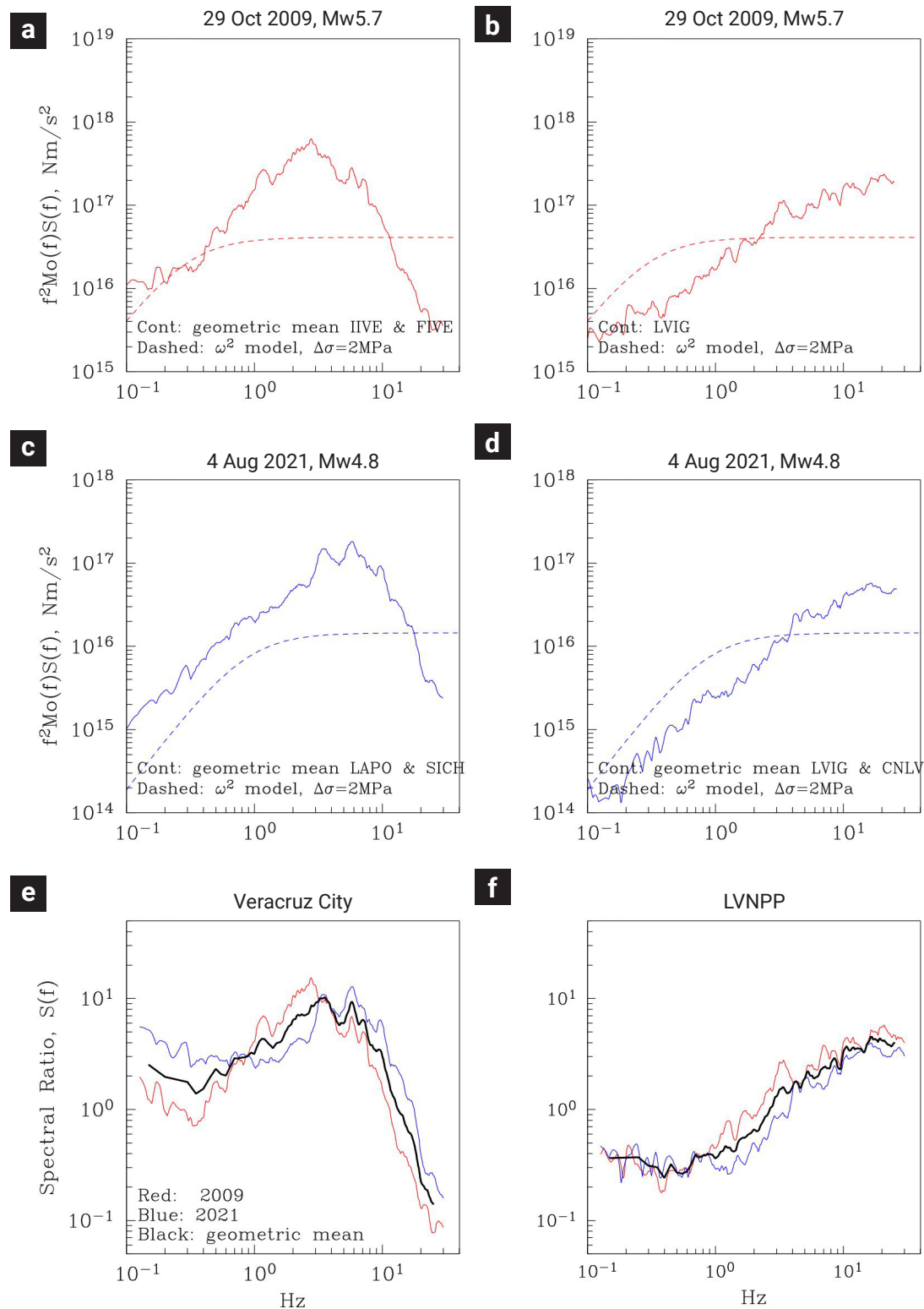
Figure 11. Geometric mean of *ASAS(f)* for the 2009 earthquake a) at the sedimentary Veracruz sites of IIVE and FIVE, b) at LVIG. Geometric mean of *ASAS(f)* for the 2021 earthquake c) at sedimentary Veracruz sites of LAPO and SICH, d) at LVIG and CNLV. Theoretical spectrum for ω^2 source model with $\Delta\sigma$ of 2 MPa are shown in a), b), c), and d). *S(f)*, the ratio of geometric mean of *ASAS(f)* to the theoretical spectrum, for the sedimentary sites in the city of Veracruz and sites in the LVNPP are shown in d) and f), respectively.

overlie a granitic inclusion. It is probably one of the harder sites of the national seismological and accelereographic networks. The low *ASAS(f)* at LVIG during the 2009 and 2021 earthquakes, of course, can not be attributed to mantle wedge. It is most likely due to the highly competent rock site where the station is situated. For certain group of events both low-*Q* mantle wedge and hard LVIG site may be responsible for low observed spectrum and lower than expected *PGA* and *PGV*. We searched for *Q(f)* which will bring the source spectra retrieved from the LVNPP recordings to theoretical source spectra (Figure 11). As intuitively expected, it requires low *Q(f)*, ~50*f*, for f < 2.5 Hz, and high *Q(f)*, ~300*f*, for f ≥2.5 Hz. A thorough study is warranted

to pin point the cause of the abnormal spectra at LVNPP. This is beyond the scope of this paper.

Conclusions

The 2009 Alvarado (M_w 5.7) and 2021 Veracruz (M_w 4.8) earthquakes are the first two moderate events to occur near the margin of southwest Gulf of Mexico that were well-recorded at local and regional distances. This permitted us to perform centroid moment tensor inversion using the *W*-phase which yielded reverse-faulting focal mechanism for both events. This
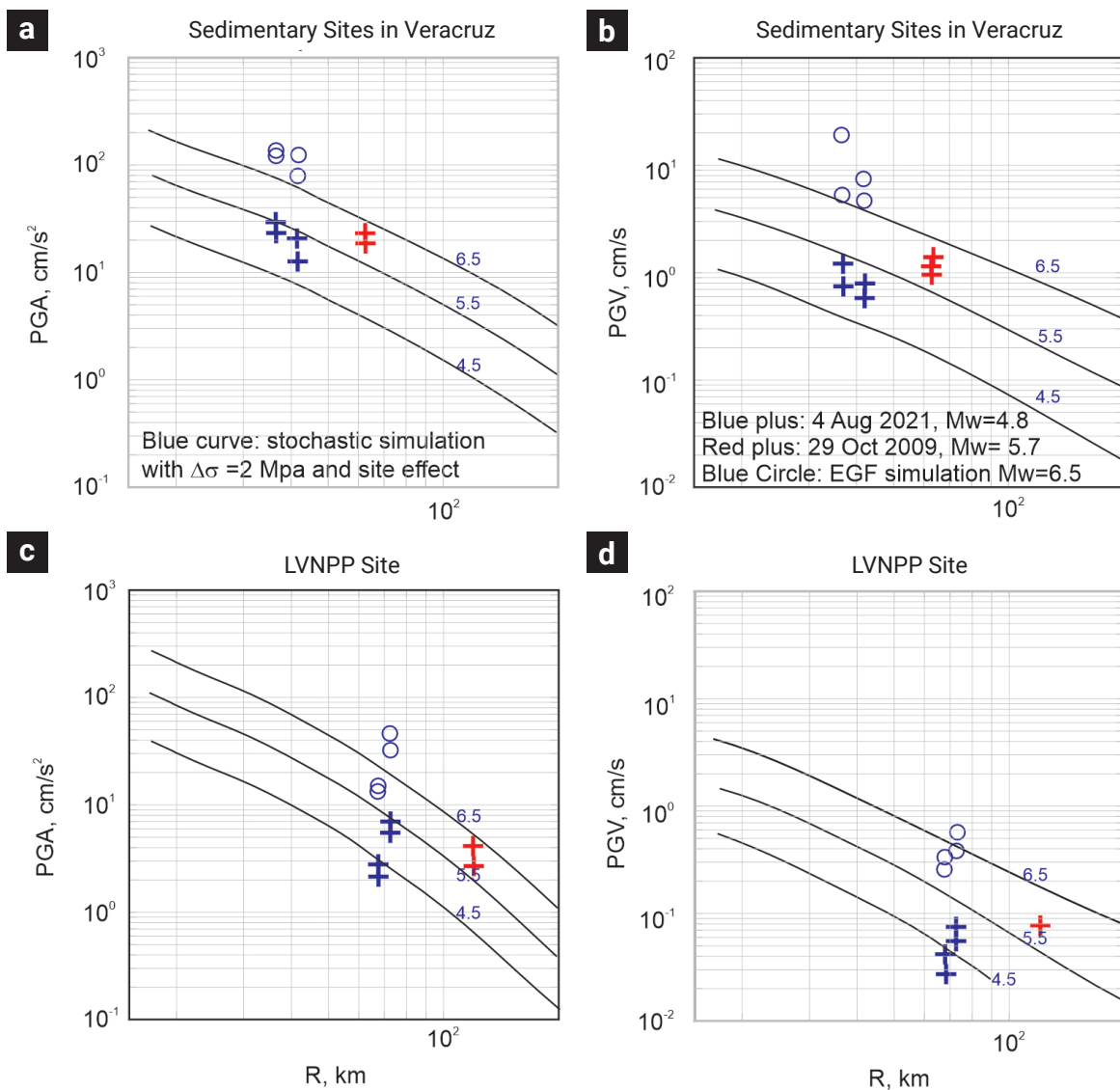

Figure 12. Predicted *PGA* curves from stochastic method for M_w 4.5, 5.5, and 6.5 earthquakes as function of *R* at a) sedimentary Veracruz sites, and c) LVNPP sites The corresponding *PGV* curves are given in b) and d). Observed values during the 2009 (red plusses) and 2021 earthquakes (blue plusses) are superimposed on these figures. Synthesized *PGA* and *PGV* values for an M_w 6.5 earthquake from the EGF technique are shown by circles.

mechanism is similar to those of three other earthquakes in the southwestern Gulf of Mexico. We also determined the focal mechanism of another earthquake (15 Feb 2017, M_w 4.3) with epicenter near the 2021 event. The mechanism of this event, strike slip, is consistent with left-lateral, strike-slip Veracruz fault on which it may have occurred. Presently, focal mechanisms of seven earthquakes along the southwestern margin of the gulf is known; of these two are strike-slip and the rest are thrust type. Thus, the stress regime near the southwest margin of the gulf appears to be more heterogeneous than previously thought.

The recordings of the 2009 and 2021 earthquakes also permitted us to estimate ground motion from future earthquakes occurring in the southwest margin of the gulf, critical for seismic risk assessment of the region but still lacking at present. In particular, the estimation of ground motion from a "migrating" M_w 6.5 earthquake has been of great concern in the seismic design of the Laguna Verde Nuclear Power Plant (LVNPP). Source spectrum computed at each station (distance $\leq$ 400 km) individually by applying reasonable Q and geometric spreading corrections, exhibits remarkably high variability due to difference in the path and local site effects. The geometric mean apparent source spectrum of both earthquakes may be modeled by an ω^2-Brune source with $\Delta\sigma = 40$ MPa. This source spectrum, along with the application of the stochastic method, yields *PGA* and velocity *PGV* as a function of distance in general agreement with the observations.

Of greater, practical importance is the estimation of ground motion at near-source sedimentary sites in the city of Veracruz and at the LVNPP. We used both EGF and stochastic methods in the estimation. The recordings of the 2021 earthquake were taken as EGFs and $\Delta\sigma$ of 2 Mpa for the EGF and target events was assumed in the simulation. While this stress drop is reasonable, it is weakly constrained by the data. In the application of stochastic method, we estimated the site effect in the city of Veracruz and at LVNPP from the spectral ratio of observed apparent source spectrum to theoretical source spectrum corresponding to the ω^2 - Brune source with $\Delta\sigma = 2$ MPa.

For an M_w 6.5 earthquake, the predicted *PGA* and *PGV* at sedimentary coastal sites above the hypocenter ($R = 20$ km) are 0.18 g and 10 cm/s. At LVNPP, the corresponding predicted motions are 0.21 g and 3 cm/s. These values may be off by a factor of 2 or more due to uncertainty in the stress drop of the postulated event. It is worth remembering that the estimates are based on few data presently available and several assumptions, e.g., ω^2 - Brune source with $\Delta\sigma = 2$ MPa is valid for all earthquakes and farfield, point source approximation holds even for an M_w 6.5 earthquake at a distance of 20 km. Thus, the estimated motions are necessarily preliminary that would be revised and modified as more near-source recordings become available.

The present study brings in to focus the need for more intensive instrumentation in the region and lays ground for future work.

References

Allmann, B. P., and P. M. Shearer (2009). Global variations of stress drop for moderate to large earthquakes, *J. Geophys. Res.*, 114, B01310. doi: **https://doi.org/10.1029/2008JB005821**

Andreani, L., Rangin, C., Martinez-Reyes, J., Le Roy, C., Aranda-Garcia, M., Le Pichon, X., Peterson-Rodriguez, R. (2008). The Neogene Veracruz Fault: evidences for left-lateral slip along the Southern Mexico Block, *Bulletin de la Société Géologique de France*, 179, 195-208. doi: **https://doi.org/10.2113/gssgfbull.179.2.195**

Boore, D. M. (1983). Stochastic simulation of high-frequency ground motions based on seismological models of radiated spectra. *Bulletin of Seismological Society of America*, 73, 1865-1884. **https://doi.org/10.1785/BSSA07306A1865**

Boore, D.M. (2003). Simulation of ground motion using the stochastic method. Pure and Applied Geophysics, 160, 635-676. **https://link.springer.com/article/10.1007/PL00012553**

Brune, J. N. (1970). Tectonic stress and the spectra of seismic shear waves from earthquakes. *Journal of Geophysical Research*, 75(26), 4997-5009. doi: **https://doi.org/10.1029/jb075i026p04997**

Canas, J. A. (1986). Estudio de factor inelástico Q de la coda de los terremotos correspondientes a las regiones central y oriental del eje volcánico de México, *Geofísica Internacional*, 25, 503-520. doi: **https://doi.org/10.22201/igeof.00167169p.1986.25.4.775**

Chael, E. P. (1987). Spectral scaling of earthquakes in the Miramichi region of New Brunswick. *Bulletin of the Seismological Society of*

America, 77(2), 347-365. doi: **https://doi.org/10.1785/bssa0770020347**

Dewey, J.W., Suárez, G. (1991). Seismotectonics of middle America, in Slemmons, D.B., Engdahl, E.R., Zoback, M.D., and Blackwell, D.D., eds., Neotectonicas of North America, Boulder, Colorado, *Geological Society of America*, Decade Map, V. 1, 309-321. doi: **https://doi.org/10.1130/DNAG-CSMS-NEO.309**

Dreger, D.S., 2003, TDMT_INV: time domain seismic moment tensor inversion, in Lee, W.H.K., Kanamori, H., Jennings, P.C., Kisslinger, C. (eds.), *International handbook of earthquake and engineering seismology*, B: London, U.K. Academic Press, 1627.

Dreger, D. S., Helmberger, D. V. (1993). Determination of source parameters at regional distances with three-component sparse network data. *Journal of Geophysical Research: Solid Earth, 98*(B5), 8107-8125. doi: **https://doi.org/10.1029/93jb00023**

Duputel, Z., Rivera, L., Kanamori, H., Hayes, G. (2012). W-phase fast source inversion for moderate to large earthquakes (1990 - 2010). *Geophysical Journal International*, 189(2), 1125-1147. doi: **https://doi.org/10.1111/j.1365-246X.2012.05419.x**

Figueroa, J. (1964). El macrosismo de Jáltipan. 1. Sismologia. Ingeniería, July, 357-362.

Franco, S. I., Canet, C., Iglesias, A., Valdés-González, C. (2013). Seismic activity in the Gulf of Mexico. A preliminary analysis. *Boletín de la Sociedad Geologíca Mexicana*, 65, 447-455. ISSN: 1405-3322.

Frohlich, C. A. (1982). Seismicity of the central Gulf of Mexico. *Geology*, 10(2), 103. doi: **https://doi.org/10.1130/0091-7613(1982)10**

Fukuyama, E., Dreger, D. S. (2000). Performance test of an automated moment tensor determination system for the future "Tokai" earthquake. *Earth, Planets and Space, 52*(6), 383-392. doi: **https://doi.org/10.1186/bf03352250**

Hayes, G. P., Rivera, L., Kanamori, H. (2009). Source Inversion of the W-Phase: Real-time Implementation and Extension to Low Magnitudes. Seismological Research Letters, 80(5), 817-822. doi: **https://doi.org/10.1785/gssrl.80.5.817**

Herrmann, R. B. (1985). An extension of random vibration theory estimates of strong ground motion at large distances. *Bull. Seism. Soc. Am., 75*, 1447-1453. doi: **https://doi.org/10.1785/BSSA0750051447**

Kanamori, H., Rivera, L. (2008). Source inversion of W phase: speeding up seismic tsunami warning. *Geophysical Journal International, 175*(1), 222-238. doi: **https://doi.org/10.1111/j.1365-246x.2008.03887.x**

Nuttli, O. W. (1983). Average seismic source-parameter relations for midplate earthquakes. *Bulletin of the Seismological Society of America, 73*(2), 519-535. doi: **https://doi.org/10.1785/bssa0730020519**

Ordaz, M., Arboleda, J., Singh, S.K. (1995). A scheme of random sum-

mation of an empirical Green's function to estimate ground motions from future large earthquakes. *Bull. Seism. Soc. Am.*, 85, 1635-1647. doi: **https://doi.org/10.1785/BSSA0850061635**

Pérez-Campos, X., Espíndola, V. H., Pérez, J. *et al.* (2019). Servicio Sismológico Nacional, Mexico. *Summary of the Bulletin of the International Seismological Centre, 53*(II), 29-40. doi: **https://doi.org/10.31905/sz7rybtm**

Reséndiz, D. (1964). El macrosismo de Jáltipan. 2. Suelos. *Ingeniería,* July, 362-379.

Rosenblueth, E. (1964). El macrosismo de Jáltipan. Introducción. Ingeniería, July, 357.

Shapiro, N. M., Singh, S. K., Iglesias-Mendoza, A., Cruz-Atienza, V. M., Pacheco, J. F. (2000). Evidence of low Q below Popocatépetl Volcano, and its implication to seismic hazard in Mexico City. *Geophysical Research Letters, 27*(17), 2753-2756. doi: **https://doi.org/10.1029/1999gl011232**

Singh, S.K., Pacheco, J.F., Garcia, D., Iglesias, A. (2006). An estimate of shear-vave Q of the mantle wedge in Mexico, *Bulletin of the Seismological Society of America*, 96, 176–187, doi: **https://doi.org/10.1785/0120050001**

Singh, S. K., Iglesias, A., García, D., Pacheco, J. F., Ordaz, M. (2007). Q of Lg Waves in the Central Mexican Volcanic Belt. *Bulletin of the Seismological Society of America*, 97(4), 1259-1266. doi: **https://doi.org/10.1785/0120060171**

Singh, S.K., Pacheco, J. F., Pérez-Campos, X., Ordaz, M., Reinoso, E. (2015). The 6 September 1997 (Mw4.5) Coatzacoalcos-Minatitlan, Veracruz, Mexico earthquake: implications for tectonics and seismic hazard of the region, *Geofísica International*, 54, 289-298. doi: **https://doi.org/10.1016/j.gi.2015.08.001**

Singh, S.K., Arroyo, D., Pérez-Campos, X., Iglesias, A., Espíndola, V.H., Ramírez, L. (2017). Guadalajara, Mexico, earthquake sequence of December 2015 and May 2016: source, Q, and ground motions, *Geofísica Internacional*, 56-2, 173-186. doi: **https://doi.org/10.22201/igeof.00167169p.2017.56.2.1764**

Suárez, G., López, A. C. G. (2015). Seismicity in the southwestern Gulf of Mexico: evidence of active back arc deformation. *Revista Mexicana de Ciencias Geológicas*, 32(1), 77-83. **http://www.redalyc.org/pdf/572/57237105007.pdf**

Suárez, G. (2000). Reverse faulting in the Isthmus of Tehuantepec: Back-arc deformation induced by the subduction of the Tehuantepec ridge, in Delgado, H., Aguirre, G., Stock, J., (eds), Cenozoic Tectonics and Volcanism of Mexico, *Geological Society of. America Special Paper*, 334, 263-268. doi: **https://doi.org/10.1130/0-8137-2334-5.263**

Appendix A

Location and moment tensor inversion of the 15 February 2017 earthquake

The 2017 earthquake was located using phase data and crustal structure given in Table 2 and varying the depth (H). Residuals as a function of H, illustrated in Figure Aa, suggest a depth between 15 and 21 km.

An Automated Moment Tensor Determination (AMTD) algorithm, developed at the Berkeley Seismological Laboratory (Fukuyama and Dreger, 2000; Dreger, 2003) and implemented at UNAM using realtime data from SSN stations (Franco *et al.*, 2013) was used to determine moment tensor of the 2017 event. Full three-component broadband displacement waveforms were inverted to obtain the moment tensor solution (Dreger and Helm-berger, 1993). The algorithm searches for the H that provides the best fit between the observed and synthetic seismograms, i.e., that H which provides greatest variance reduction (VR). VR as a function of H is shown in Figure Ab. We note that the focal mechanism remains stable for sources at H between 10 km and 40 km and VR is relatively insensitive to H between 20 and 35 km. Thus, from AMTD a depth between 20 and 35 km is acceptable. Since H = 20 km is in agreement with the location output, we take this to be depth of the 2017 event. Figure Ac compares the observed and synthetic displacements (H = 18 km) at 4 stations. The fit is good. M_0 is 2.15×10^{15} Nm (M_w4.3) and the focal mechanism is given by:

Nodal plane 1: $\varphi_1 = 3090$, $\delta_1 = 74^0$, $\lambda_1 = 23^0$
Nodal plane 2: $\varphi_2 = 2120$, $\delta_2 = 67^0$, $\lambda_2 = 163^0$
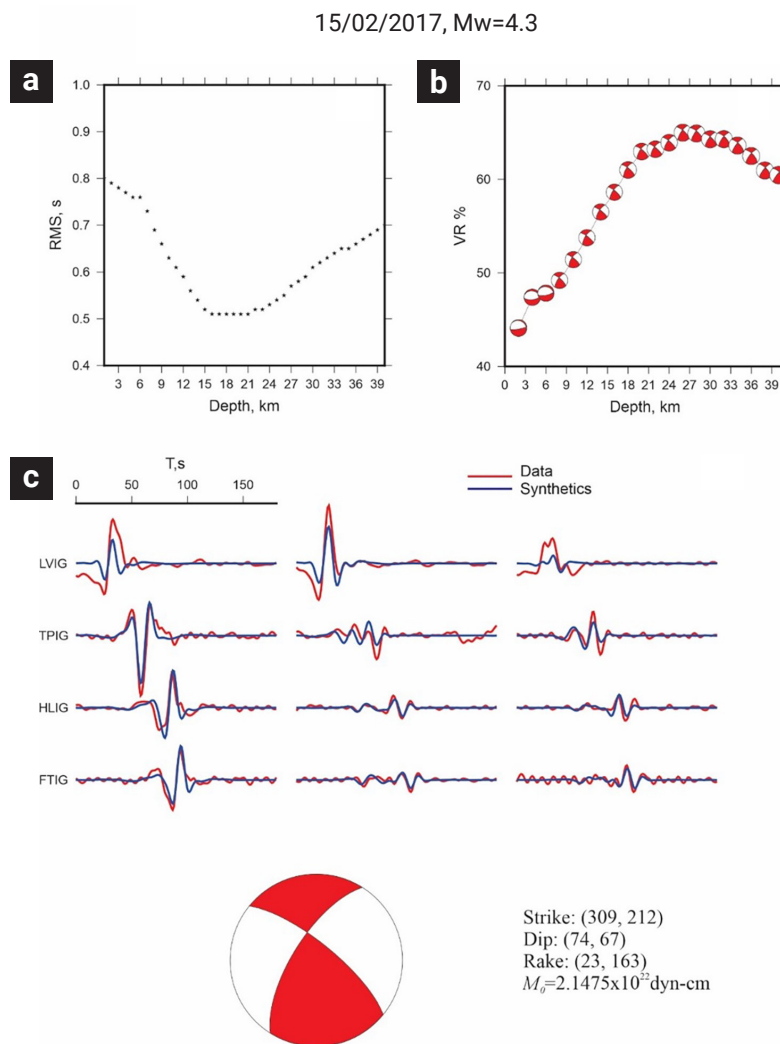
15/02/2017, Mw=4.3

Figure A. a) RMS error as a function of depth, *H*, from earthquake location program. Minimum in the plot suggests *H* between 15 and 21 km. b) Variance reduction (*VR*) as a function of *H*. Although the focal mechanism is stable, *H* is poorly resolved from VR. c) Observed (red) and synthetic (blue) (*H* = 20 km) displacements at four broadband stations. Red and white beach ball shows the focal mechanism of the 2017 earthquake.